https://doi.org/10.1016/j.jmst.2021.07.016

Enhanced ferroelectric polarization with less wake-up effect and improved endurance of $Hf_{0.5}Zr_{0.5}O_2$ thin films by implementing W electrode

Dao Wang[a], Yan Zhang[a], Jiali Wang[a], Chunlai Luo[a], Ming Li[a], Wentao Shuai[a], Ruiqiang Tao[a], Zhen Fan[a], Deyang Chen[a, b], Min Zeng[a], Jiyan Dai[b, *], Xubing Lu[a, **], J.-M. Liu[c]

[a]Guangdong Provincial Key Laboratory of Quantum Engineering and Quantum Materials and Institute for Advanced Materials, South China Academy of Advanced Optoelectronics, South China Normal University, Guangzhou, 510006, PR China

[b]Department of Applied Physics and Materials Research Center, The Hong Kong Polytechnic University, Hung Hom, Kowloon, Hong Kong, P. R. China

[c]Laboratory of Solid State Microstructures and Innovation Centre of Advanced Microstructures, Nanjing University, Nanjing, 210093, PR China

[*]Corresponding author.
E-mail address: jiyan.dai@polyu.edu.hk (J. Y. Dai)
[**]Corresponding author.
E-mail address: luxubing@m.scnu.edu.cn (X. B. Lu)

Keywords: $Hf_{0.5}Zr_{0.5}O_2$ films; ferroelectric polarization; endurance properties; thermal expansion coefficient; W electrode

Abstract

This paper reports the improvement of electrical, ferroelectric and endurance of $Hf_{0.5}Zr_{0.5}O_2$ (HZO) thin film capacitors by implementing W electrode. The W/HZO/W capacitor shows excellent pristine 2 P_r values of 45.1 μC/cm^2 at ±6 V, which are much higher than those of TiN/HZO/W (34.4 μC/cm^2) and W/HZO/TiN (26.9 μC/cm^2) capacitors. Notably, the maximum initial 2 P_r value of W/HZO/W capacitor can reach as high as 57.9 μC/cm^2 at ±7.5 V. These strong ferroelectric polarization effects are ascribed to the W electrode with a fairly low thermal expansion coefficient which provides a larger in-plane tensile strain compared with TiN electrode, allowing for enhancement of o-phase formation. Moreover, the W/HZO/W capacitor also exhibits higher endurance, smaller wake-up effect (10.1%) and superior fatigue properties up to 1.5×10^{10} cycles compared to the TiN/HZO/W and W/HZO/TiN capacitors. Such improvements of W/HZO/W capacitor are mainly due to the decreased leakage current by more than an order of magnitude compared to the W/HZO/TiN capacitor. These results demonstrate that capping electrode material plays an important role on the enhancement of o-phase formation, reduce oxygen vacancies, mitigate wake up effect and improve reliability.

1. Introduction

$Hf_{0.5}Zr_{0.5}O_2$ (HZO) thin film is one of the most attractive candidates among various cation-doped HfO_2 ferroelectric thin films [1]. The ferroelectricity in HfO_2 film originates from the non-centrosymmetric orthorhombic phase (o-phase, space group $Pca2_1$) [2]. It has been reported that the generation and stability of o-phase are closely related to the mechanical clamping strain exerted by the capping layers (or top electrodes), whereas the magnitude of strain depends on the difference in thermal expansion coefficient (TEC) between the top and bottom electrodes or between the electrodes and ferroelectric films [3-8]. To achieve high ratio/stability of o-phase in HZO films, various capping layer materials such as TiN [1, 2, 7], TaN [9, 10, 11], Pt [3, 4], W [3, 5], Ru [6], RuO_2 [7], Co [12], Ni [13], Au [14], VO_x [15], HfN [16], and Al_2O_3 [17] etc. have been extensively investigated. Currently, TiN is widely adopted as capping electrode to induce ferroelectricity in HZO-based capacitors. However, it has a high TEC (9.1×10^{-6} K^{-1}) [7] comparable with that of HZO film (10×10^{-6} K^{-1}) [18], which is not beneficial for suppression of non-ferroelectric (i.e., c, t, and m) phases, resulting in relatively low ferroelectric polarization. In addition, the interface chemistry of the capping electrodes/HZO films is also an essential factor that affects their electrical, ferroelectric and endurance of HZO-based ferroelectric capacitors [19, 20, 21]. For TiN electrode, it is a reactive metal that could easily react with oxygen in HZO layer, leading to generation of oxygen vacancies inside HZO film and the formation of the non-ferroelectric dead layer at the interfacial region [7]. These defects can cause high leakage current, strong wake up effect and poor reliability of HZO-based ferroelectric capacitors [20, 21].

To overcome these disadvantages of TiN, it is a critical issue to choose appropriate electrode materials to improve the ferroelectric and endurance properties of HZO films. As a possibly eligible capping electrode, tungsten (W) exhibits the lowest TEC (4.5×10^{-6} K^{-1}) [3] among the extensively employed metal electrodes. It can produce a high in-plane tensile strain during the annealing process, which favors the formation of o-phase while the generation of m-phase is suppressed. Furthermore, W electrode has high chemical stability [5], which can lessen the reaction with the HZO film and decrease the vacancy defects of the HZO film, resulting in lowered leakage current, strengthened breakdown field and improved stability of its polarization states during field cycling.

In this work, we performed a comparative investigation on the electrical, ferroelectric and endurance properties of HZO film with two different electrodes, TiN and W. These findings indicate that HZO film with W top and bottom electrodes present significantly increased polarization value, obviously decreased leakage current, mitigated wake-up effect, and clearly enhanced endurance properties.

2. Experiments

2.1. Preparation

The three different structures of W/HZO/W, TiN/HZO/W and W/HZO/TiN capacitors were fabricated; abbreviated as WW, TW and WT capacitors, respectively. The first letters in WW, TW and WT represent bottom electrode in the capacitors. The key process flow for the three types of capacitors is illustrated in Fig. 1(a). First, for WW, TW and WT capacitors, the W and TiN bottom electrodes with a thickness of 80

and 50 nm were deposited on Si (100) substrates by using sputtering, respectively. Next, 15 nm-thick HZO films were deposited by atomic layer deposition (ALD) at 280 ℃ with Hf: Zr=1:1 cycle ratio. $Hf[N(CH_3)_2]_4$, $Zr[N(CH_3)_2]_4$ and O_3 were used as Hf precursor, Zr precursor and oxygen source, respectively. Then, the different top electrodes (80 nm for W or 50 nm for TiN) were sputtering deposited onto HZO films as a contact pad through a shadow mask with a 100 μm hole diameter. Finally, all the capacitors were crystallized by rapid thermal annealing (RTA) at 550 ℃ in a N_2 atmosphere for 30 s.

2.2. Characterization

For electrical characterization, the FE, dielectric, and leakage current properties were measured with Radiant Precision, Agilent B1500A semiconductor product analyzer, and E4990A impedance analyzer, respectively. The crystal structures of HZO film with various electrodes were examined by grazing incidence X-ray diffraction (GIXRD, PANalytical X' Pert Pro diffractometer) with an incidence angle of 0.5°. The microstructures of HZO film and top/bottom interfaces were investigated by high resolution transmission electron microscope (HRTEM, JEM2100F) using a cross-section specimen.

3. Results and Discussion

Figures 1(b) and (c) exhibit the cross-sectional HRTEM images of the WW and WT capacitors. The lattice fringes in various directions were observed for the HZO films, meaning that the films are polycrystalline. For WW capacitor, both the top and bottom interfaces are clean and uniform, implying that the interfaces between HZO

films and W electrodes is chemically stable. However, the top TiN/HZO interface in WT capacitor is very obscure and uneven, suggesting that strong interface reaction or interaction should occur between top TiN and HZO film.

To analyze the influence of different top and bottom electrodes on crystalline characteristics of the annealed HZO films, GIXRD scanning was performed in the two theta (2 θ) range of 25°~33°, as shown in Fig. 2(a). The noticeable diffraction peaks appear at 28.5° and 31.6°, corresponding to the (−111) and (111) reflections of m-phase [1, 2], are detected for the WT capacitor, but are weakened for the TW capacitor. No peaks can be observed in the WW capacitor near 28.5° and 31.6°, suggesting that the m-phase is well suppressed. Additionally, the highest intensity peak observed in the three types of capacitors near 30.5° are designated as the combination of the o (111) and t (011) phases due to their structural similarities [4]. The peak position of o-/t-phase for WW capacitor is slightly shift toward lower angle than that of the TW and WT capacitors (as depicted from Fig. 2 (b)), which is assumed to be attributed to elongated d-spacing in the HZO film of WW capacitor [22]. The GIXRD spectra of the three capacitors are fitted by Gaussian function as seen in the Figs. 2(c) and S1 (see Fig. S1 in the supplementary material). The relative ratio of each phase that acquired by integrating the area of each Gaussian peak [4] is shown in Fig. 2(d) for the WW, TW and WT capacitors. The relative ratio of o (111) / t (011) phase in WW capacitor is 87.1%, which is much higher than those of TW (76.2%) and WT (69.2%) capacitors. These results were due to the different in-plane strains applied to the HZO film by the W and TiN electrodes with various TEC [3].

The in-plane strain was calculated by $\varepsilon_T(T_A)=(\alpha_{film}-\alpha_{cap})\times(T_A-T_{RT})$ [23, 24, 25], where the α_{film} and α_{cap} are the TEC of the HZO films and capping materials, respectively; T_A and T_{RT} are the annealing and room temperatures, respectively. The values of 4.5×10^{-6} K^{-1}, 9.1×10^{-6} K^{-1}, 10×10^{-6} K^{-1}, 25 °C and 550 °C are used for α_W, α_{TiN}, α_{HZO}, T_{RT} and T_A, respectively. Consequently, the ε_T values were calculated to be about 0.289%, and 0.047% for the W and TiN capping electrodes, respectively. It is confirmed that W with lower TEC can produce a stronger in-plane tensile strain, allowing generation of m-phase to be inhibited and formation of o-phase to be enhanced [26].

To investigate the effects of various electrodes on the ferroelectric polarization characteristics, the pristine polarization-voltage (P-V) loops were measured at an applied voltage varying from ±1 V to ±7.5 V and a frequency of 10 kHz. Figs. 3(a), (b) and (c) show well saturated P-V loops of the three types of capacitors, revealing their good ferroelectricity. The saturation polarization (P_s), remanent polarization (2 P_r) and coercive voltage (2 V_c) values of the three capacitors increase with increasing applied voltage as depicted in Figs. 3(d), (e) and (f), respectively. From Figs. 3(d) and (e), it can be clearly observed that the P_s and 2 P_r values of the WW capacitor over the entire voltage range are higher compared with those of the TW and WT capacitors. The P_s and 2 P_r values of WW capacitor are approximately 34.9 μC/cm^2 and 45.1 μC/cm^2 at a voltage of ±6 V, much higher than those of TW (30.8 and 34.4 μC/cm^2) and WT (22.1 and 26.9 μC/cm^2) capacitors. Notably, the maximum P_s and 2 P_r values of WW capacitor can reach as high as 41.6 μC/cm^2 and 57.9 μC/cm^2 at ±7.5 V. Additionally,

the WW capacitor exhibits a lower 2 V_c with applied voltage over 3 V compared to that of the TW and WT capacitors; this low coercive voltage allows for the use of a lower applied voltage to drive the cycling tests (Fig. 3(f)). To correct for leakage and possible contributions from parasitic charges, the positive-up negative-down (PUND) method [5] was used to obtain the intrinsic P_r. The P-V loops acquired from the PUND method (Fig. 3(g)) showed the intrinsic 2 P_r value of approximately 43.1, 30.9 and 21.1 $\mu C/cm^2$ at ±5 V for WW, TW and WT capacitors, respectively. The high o/t-phase ratio of WW capacitor was already confirmed by GIXRD (Fig.2(d)), which is considered to be a primary reason for its robust ferroelectricity. The quality of the interfacial layer between electrodes (TiN and W) and HZO films could be another important factor influencing the ferroelectric polarization [21]. To examine the electrical properties of these three types of capacitors, Fig. 3(h) reveals the virgin leakage current (J-V) characteristics measured at voltage of ±4 V. Note that clear current peaks were observed for both WW and TW capacitors, which is believed to be ascribed to the strong ferroelectric polarization switching induced negative differential resistance effect [17]. However, no current peaks were observed for WT capacitor, which may be attributed to the large amount of oxygen vacancies in the top HZO/TiN interface. The large concentration of mobile charged oxygen vacancies in the interface defective HZO layer screens the polarization charges and leads to the weak response to the polarization switching, eventually resulting in much smaller charge redistribution at the top interface [27]. The current density of WW capacitor is approximately 7.9×10^{-5} A/cm^2 at +4 V, much lower than those of TW (4.6×10^{-4}

A/cm^2) and WT (1.4×10^{-3} A/cm^2) capacitors. Particularly, the leakage current of WW capacitor is reduced by more than one order of magnitude compared to the WT capacitor, which helps to improve durability. The difference of leakage current between WW, TW and WT capacitors could be ascribed to the following reasons: First, for TW capacitor, the bottom TiN electrode is already partially oxidized during the ALD process owing to the oxygen source injection, whereas the top TiN electrode for WT capacitor was not exposed to the oxygen source because it was deposited after the sputtering process [19, 21, 27]. During the crystallization annealing process, the chemical reduction of the HZO film is expected to generate a lower amount of oxygen vacancies at the bottom TiN/HZO interface in TW capacitor compared to the top HZO/TiN interface in WT capacitor [19, 21, 27]. Because the bottom TiN electrode is already partially oxidized at the interface, the oxygen scavenging effects at the bottom TiN/HZO interface in TW capacitor is much weaker than that at the top HZO/TiN interface in WT capacitor [19, 21, 27]. So, compared with the WT capacitor, the TW capacitor exhibits a lower leakage current due to lower oxygen vacancies. Secondly, the leakage current of the WW capacitor is the lowest among these three capacitors. This is because that the negative standard heat of formation of WO_x is larger (−201.4 kcal/mol for WO_3 and −140.9 kcal/mol for WO_2) [28] as compared with that of TiO_x (−105.6~−154.9 kcal/mol) [29]; this can reduce the interfacial reaction between W and HZO film. Additionally, for WT and TW capacitors, Ti or N could diffuse from the TiN electrode into the HZO layer after annealing; this can be avoided in the case of WW capacitor [6]. Thirdly, the work function of W (4.55 eV) [30] is similar to that

of TiN (4.2~4.5 eV) [7, 31, 32], but the TiN electrode is easily to be oxidized into TiO_xN_y and takes oxygen away from the HZO film, leading to a decrease of the Schottky barrier height for electrons. These facts may result in a relatively large amounts of defects and vacancies in the TW and WT capacitors, leading to the polarization charges to be screened and leakage current increased. However, the interface reactions and the diffusion of electrode atoms may be decreased by the HZO with W top and bottom electrodes. Thus, these excellent electrical and ferroelectric properties of WW capacitor are also attributed to less defects and vacancies.

Figures 4(a)-(c) and (d)-(f) show the evolution of P-V and switching current-voltage (Is-V) curves of WW, TW and WT capacitors measured in pristine state and after 10^3, 10^4 and 10^5 cycles. The triangular wave with an amplitude of ±3 V and a frequency of 1 kHz is used for the electrical cycling. One can see that, the P-V loops shape of each capacitor is slanted in virgin state and the corresponding Is-V curves possesses only a single broad peak on each side of the voltage, implying that the film possesses relative homogeneity in the internal electric field and/or coercive field at initial state [20, 33]. It is worth noting that, due to its strong ferroelectricity, the height of Is peak of the WW capacitor is higher than that of the TW and WT capacitors. After 10^3 cycles, all capacitors reach a wake-up state. Their shape of the P-V loops becomes more ideally rectangularity and the 2 P_r values increase. The corresponding Is peaks, thereafter, exhibit a single narrower peak and the Is peak height increase. The changes in the $\Delta 2P_r/2P_{r,\,initial}$ ($= (2P_r - 2P_{r,\,initial})/2P_{r,\,initial}$) values of the all capacitors as a function of number of electrical switching cycles, are shown

in Fig. 4(j). The values of $\Delta 2P_r/2P_{r,\,initial}$ are 10.1%, 24.1% and 14.0% for WW, TW and WT capacitors at wake-up state, respectively. This suggests that mitigation in wake-up behavior of HZO films using top and bottom W electrodes is mainly due to the minimized formation of the dead layer at the interface.

The switchable polarization and the height of Is peaks of three capacitors progressively reduce with a further increased number of field cycles, which corresponds to the generally observed fatigue in many doped HfO_2 ferroelectrics. Note that a distortion in the P-V curves (Fig. 4(c)) and split-up of current peaks in Is-V curves (Fig. 4(f)) are observed at the positive axis for WT capacitor after 10^5 cycles, but is not the case for the WW and TW capacitors. The reason behind this phenomenon is that the switching electric field is severely lost across the high portion of m-phase and the top TiO_xN_y dead layer with low permittivity during cycling, which results in insufficient domain switching and spatial inhomogeneity defect distribution [20, 21, 34, 35].

Figs. 4(g)-(i) display the changes in the dielectric constant-voltage (ε_r-V) curves extracted from the capacitance measurement of three capacitors with different number of electrical switching cycles. All capacitors exhibit the butterfly-like feature, which is specific to ferroelectrics. Similarly, the double peaks are also observed in the ε_r-V curves for WT capacitor at the positive axis after 10^5 cycles. The ε_r values (the intersection points of the butterfly curves) of each HZO capacitor with various electrical cycles is summarized in Fig. 4(l). The WW capacitor had a ε_r value of 31.9 in the initial state, which was larger than that the TW (28.8) and WT (27.2) capacitors.

Two possible mechanisms can cause the relatively high ε_r in the WW capacitor. The first is the highest o-phase fraction, which was confirmed by the GIXRD analysis; one should consider that the ε_r of the m-phase (ε_r =16~20) is relatively smaller than that of the o-phase (ε_r =27~35) [36]. The second reason is the non-ferroelectric dead layer near the top/bottom interfaces of the WW capacitor is minimum as confirmed by the HRTEM images. Simultaneously, the variation in the leakage currents with the bipolar cycling was also detected under an applied voltage of −3 V (see Fig. S2 in the supplementary material). The current density at −3 V is plotted as a function of cycling number as presented in Fig. 4(k). It can be clearly seen that the current density of WW capacitor is significantly lower than that of TW and WT capacitors at all test conditions.

From Figs. 4(i), (k) and (l), both ε_r and leakage current decrease in the wake-up state, while the $\Delta P_r/2P_{r,\ initial}$ values increase. The ε_r decrease and $\Delta 2P_r/2P_{r,\ initial}$ increase could be related to a phase transition from t- to o-phase in the interfacial region and redistribution of oxygen vacancies [37, 38]. The leakage current during the wake-up stage slightly reduces, indicating that there is almost no generation of new defects assisting the charge transport through the trap-assisted tunneling but a redistribution of the existing ones, as well as a change of their occupancy [20]. Further cycling results in the generation of additional defects, which lead to a sharp increase of leakage current (Fig. 4(k)). This is accompanied with the degradation of P_r, continuation of the phase transition and further drop of the total capacitance and ε_r value as well.

Figure 5(a) illustrates the endurance properties of the WW, TW and WT capacitors. The endurance measurement conditions are as follows: cycling was performed with a bipolar triangular waveform of 100 kHz. The amplitude of the field cycling/PUND read pulses was set at 1.8/3 V for WT capacitor, while it was 2/3 V for WW and TW capacitors. The WT capacitor presents a prolonged wake-up effect until hard breakdown occurs after 1.5×10^{9} cycles, which may be ascribed to the fact that the HZO film with TiN top electrode has more non-ferroelectric dead layer and a larger amount of oxygen vacancies at the interface [7, 21, 27]. However, the WW capacitor exhibits better endurance up to 1.5×10^{10} cycles without breakdown, while the breakdown was observed in the TW capacitor when the electrical cycles to 4.7×10^{9} cycles. These results indicate that replacing TiN electrodes with W at the bottom and top electrodes of the HZO layer can produce better interfaces which improves the endurance properties. The leakage results shown in Fig. 3(h) infer that the W electrode can decrease interfacial reaction and oxygen vacancies [5]. Furthermore, the accelerated endurance measurement was carried out by applying a larger field cycling/PUND read pulse amplitude and lower frequency. The test condition is that the triangular waveform is used for field cycling/PUND read pulses, the amplitude is increased from 3/3 V to 6/6 V at a frequency of 10 Hz. Fig.5 (b) shows the number of endurance cycles of the three capacitors as a function of cycling voltage. Additionally, the endurance properties were also measured at 4 V cycling voltage with the frequency varying from 10 Hz to 1000 Hz. The number of endurance cycles of the three capacitors as a function of the frequency is shown in Fig. 5 (c). As

can be seen from Figs. 5(b) and (c), the endurance measurement demonstrates that the number of endurable cycles of the WW capacitor is higher than those of the TW and WT capacitors under the same cycling voltage and frequency. When the same number of breakdown cycles is 30 (Fig. 5(b)), the withstand voltage of the WW capacitor is 6 V while it is only 5 V for the WT and TW capacitors, indicating that the adoption of top and bottom W electrodes can improve breakdown immunity and endurance of HZO films. The extrapolation results of the endurance properties at different cycling voltages and frequencies suggest that the WW capacitor displays more endurance cycles compared with TW and WT capacitors under voltage higher than 1 V and frequency less than 10 MHz, manifesting that WW capacitor was more suitable for high voltage and low frequency applications [6]. Similar to endurance, the retention of the HZO-based ferroelectric capacitors also depends on the bottom and top electrodes. The retention test also was performed at ±5 V pulse amplitude with 1 ms pulse width, and Fig. 5(d) depicts normalized polarization switched charge P^*_r ($P^*_r = P_{switch} + P_{non\text{-}switch}$) values with times. After 10^4 second, it can be clearly observed that the polarization remains of the WW capacitor is 98% which is better than that of the TW (92%) and WT (88%) capacitors. Moreover, linear extrapolation in the logarithmic time scale suggests that the polarization remains is 97%, 89% and 79% after 10-years for WW, TW and WT capacitors, respectively. The worse retention properties in TW and WT capacitors can be attributed to two major reasons. One is that there may exist a depolarization field in the HZO film [7, 39, 40], which is caused by a TiO_xN_y or TiO_2 interfacial layer between the HZO film and the TiN electrode in TW and WT

capacitors. Another possible reason may be due to the interface defects like oxygen vacancy at the HZO/TiN interface[19, 31], which may also degrade the long-term retention property [40].

4. Conclusion

In conclusion, the electrical, wake-up effect and reliability characteristics of HZO film are found to be influenced by W and TiN electrode with different TEC values which control the type of strain and the amount of oxygen vacancy inside HZO film. Our results suggest that the HZO film with both top and bottom W electrodes exhibit the strongest ferroelectricity with a large proportion of o-phase and an improved initial 2 P_r of 57.9 $\mu C/cm^2$. This is attributed to the fact that W with a relatively low TEC can produce a larger in-plane tensile strain during RTP, resulting in distinctly suppressed m-phase and strengthened formation of o-phase. In addition, the WW capacitor is found to present better electrical properties than those of TW and WT capacitors. Consequently, the mitigative wake up effect, good endurance properties and long retention have also been demonstrated in WW capacitor. This work indicates that the W electrode with comparatively low TEC and high thermal stability can provide an effective way to stabilize more o-phases and lower oxygen vacancies, so as to achieve highly reliable HZO-based ferroelectric capacitors that are crucial for various memory applications.

Acknowledgments

This work was supported by National Natural Science Foundation of China (Grant No. 51872099), Hong Kong Research Grant Council (Grant No. 15300619),

and Science and Technology Program of Guangzhou (Grant No.201905-0001). Y. D. C. acknowledges the financial support by the Hong Kong Scholars Program (Grant No. XJ2019006). X. B. L. and Z. F. acknowledge the support of the Project for Guangdong Province Universities and Colleges Pearl River Scholar Funded Scheme (2016 and 2018).

References

[1] J. Müller, T. S. Böscke, U. Schröder, S. Mueller, D. Bräuhaus, U. Böttger, L. Frey, T. Mikolajick, Nano. Lett. 12 (2012) 4318-23.

[2] X. H. Sang, E. D. Grimley, T. Schenk, U. Schröder, J. M. LeBeau, Appl. Phys. Lett. 106 (2015) 162905.

[3] R. R. Cao, Y. Wang, S. J. Zhao, Y. Yang, X. L. Zhao, W. Wang, X. M. Zhang, H. B. Lv, Q. Liu, M. Liu, IEEE. Electron. Device. Lett. 39 (2018) 1207-1210.

[4] Y. C. Lin, F. McGuire, A. D. Franklina, J. Vac. Sci. Technol. B. 36 (2018) 011204.

[5] G. Karbasian, R. Reis, A. Yadav, A. Tan, C. Hu, S. Salahuddin, Appl. Phys. Lett. 111 (2017) 022907.

[6] R. R. Cao, B. Song, D. S. Shang, Y. Yang, Q. Luo, S. Y. Wu, Y. Li, Y. Wang, H. B. Lv, Q. Liu, M. Liu, IEEE. Electron. Device. Lett. 40 (2019) 1744-1747.

[7] Y. Goh, S. H. Cho, S. H. K. Park, S. Jeon, Nanoscale. 12 (2020) 9024-9031.

[8] Z. Wen, X. B. Qiu, C. Li, C. Y. Zheng, X. H. Ge, A. D. Li, D. Wu, Appl. Phys. Lett. 104 (2014) 042907.

[9] P. D. Lomenzo, Q. Takmee, C. Z. Zhou, C. M. Fancher, E. Lambers, N. G. Rudawski, J. L. Jones, S. Moghaddam, T. Nishida, J. Appl. Phys. 117 (2015) 134105.

[10] W. W Xiao, C. Liu, Y. Peng, S. Z. Zheng, Q. Feng, C. F. Zhang, J. C. Zhang, Y. Hao, M. Liao, Y. C. Zhou, ACS Appl. Electron. Mater. 1 (2019) 919-927.

[11] Y. Peng, W. W. Xiao, G. Q. Han, J. B. Wu, H. Liu, Y. Liu, N. Xu, T. J. K. Liu, Y. Hao, IEEE. Electron. Device. Lett. 40 (2019) 9-12.

[12] Y. F. Wei, S. Matzen, C. P. Quinteros, T. Maroutian, G. Agnus, P. Lecoeur, B. Noheda, npj. Quantum. Mater. 4 (2019) 1-6.

[13] X. Zhang, L. Chen, Q. Q. Sun, L. H. Wang, P. Zhou, H. L. Lu, P. F. Wang, S. J. Ding, D. W. Zhang, Nanoscale. Res. Lett. 10 (2015) 25.

[14] L. Q. Tu, R. R. Cao, X. D. Wang, Y. Chen, S. Q. Wu, F. Wang, Z. Wang, H. Shen, T. Lin, P. Zhou, X. J. Meng, W. D. Hu, Q. Liu, J. L. Wang, M. Liu, J. H. Chu, Nat. Commun. 11 (2020) 101.

[15] Y. Zhang, Z. Fan, D. Wang, J. L. Wang, Z. M. Zou, Y. S. Li, Q. Li, R. Q. Tao, D. Y. Chen, M. Zeng, X. S. Gao, J. Y. Dai, G. F. Zhou, X. B. Lu, J-M. Liu, ACS Appl. Mater. Inter. 12 (2020) 40510-40517.

[16] B. J. Zeng, W. W Xiao, J. J. Liao, H. Liu, M. Liao, Q. X. Peng, S. Z. Zheng, Y. C. Zhou, IEEE. Electron. Device. Lett. 39 (2018) 1508-1511

[17] J. L. Wang, D. Wang, Q. Li, A. H. Zhang, D. Gao, M. Guo, J. J. Feng, Z. Fan, D. Y. Chen, M. H. Qin, M. Zeng, X. S. Gao, G. F. Zhou, X. B. Lu, J.-M. Liu, IEEE. Electron. Device. Lett. 40 (2019) 1937-1940.

[18] M. H. Park, Y. H. Lee, H. J. Kim, Y. J. Kim, T. Moon, K. D. Kim, S. D. Hyun, T. Mikolajick, U. Schröder, C. S. Hwang, Nanoscale. 10 (2018) 716-725.

[19] W. Hamouda, A. Pancotti, C. Lubin, L. Tortech, C. Richter, T. Mikolajick, U. Schröder, N. Barrett, J. Appl. Phys. 127 (2020) 064105.

[20] M. Pešic´, F. P. G. Fengler, L. Larcher, A. Padovani, T. Schenk, E. D. Grimley, X. H. Sang, J. M. LeBeau, S. Slesazeck, U. Schröder, T. Mikolajick, Adv. Funct. Mater. 26 (2016) 4601-4612.

[21] M. H. Park, D. H. Lee, K. Yang, J-Y. Park, G. T. Yu, H. W. Park, M. Materano, T. Mittmann, P. D. Lomenzo, T. Mikolajick, U. Schröder, C. S. Hwang, J. Mater. Chem. C. 8 (2020) 10526-10550.

[22] Y. F. Wei, P. Nukala, M Salverda, S. Matzen, H. J. Zhao, J. Momand, A. S. Everhardt, G. Agnus, G. R. Blake, P. Lecoeur, Nat. Mater. 17 (2018) 1095-1100.

[23] T. Shiraishi, K. Katayama, T. Yokouchi, T. Shimizu, T. Oikawa, O. Sakata, H. Uchida, Y. Imai, T. Kiguchi, T. J. Konno, H. Funakubo, Mater. Sci. Semicond. Proc. 70 (2017) 239-245.

[24] T. R. Taylor, P. J. Hansen, B. Acikel, N. Pervez, R. A. York, S. K. Streiffer, J. S. Speck, Appl. Phys. Lett. 80 (2002) 1978-1980.

[25] X. F. Li, C. Li, Z. Y. Xu, Y. S. Li, Y. H. Yang, H. H. Hu, Z. Z. Jiang, J. Y. Wang, J. X. Ren, C. Y. Zheng, C. J. Lu, Z. Wen, Phys. Status. Solidi. RRL. 15 (2021) 2000481.

[26] P. Fan, Y. K. Zhang, Q. Yang, J. Jiang, L. M. Jiang, M. Liao, Y. C. Zhou, J. Phys. Chem. C. 123 (2019) 21743-21750.

[27] Y. Matveyev, D. Negrov, A. Chernikova, Y. Lebedinskii, R. Kirtaev, S. Zarubin, E. Suvorova, A. Gloskovskii, A. Zenkevich, ACS Appl. Mater. Inter. 9 (2017) 43370-43376.

[28] A. D. Mah, J. Am. Chem. Soc. 81 (1959) 1582-1583.

[29] T. V. Charlu, O. J. Kleppa, T. B. Reed, J. Chem. Thermodyn. 6 (1974) 1065-1074.

[30] H. B. Michaelson, J. Appl. Phys. 48 (1977) 4729.

[31] Y. Goh, S. H. Cho, S. H. K. Park, S. H. Jeon, IEEE. Trans. Electron. Devices, 67 (2020) 3431-3434.

[32] M. Pešić, T. Li, V. D. Lecce, M. Hoffmann, M. Materano, C. Richter, B. Max, S. Slesazeck, U. Schröder, L. Larcher, T. Mikolajick, IEEE. J. Electron. Devices. Soc. 6 (2018) 1019-1025.

[33] A. G. Chernikova, M. G. Kozodaev, D. V. Negrov, E. V. Korostylev, M. H. Park, U. Schröder, C. S. Hwang, A. M. Markeev. ACS Appl. Mater. Inter. 10 (2018) 2701-2708.

[34] M. H. Park, H. J. Kim, Y. J. Kim, W. Jeon, T. Moon, C. S. Hwang, Phys. Status. Solidi. RRL. 8 (2014) 532-535.

[35] T. Schenk, U. Schröder, M. Pešić, M. Popovici, Y. V. Pershin, T. Mikolajick, ACS Appl. Mater. Inter. 6 (2014) 19744-19751.

[36] E. D. Grimley, T. Schenk, X. H. Sang, M. Pešic´, Schröder, T. Mikolajick, J. M. LeBeau, Adv. Electron. Mater. 2 (2016) 1600173.

[37] H. J. Kim, M. H. Park, Y. J. Kim, Y. H. Lee, T. Moon, K. D. Kim, S. D. Hyun, C. S. Hwang, Nanoscale. 8 (2016) 1383-1389.

[38] S. D. Li, D. Y. Zhou, Z. X. Shi, M. Hoffmann, T. Mikolajick, U. Schröder, Adv. Electron. Mater. 6 (2020) 2000264.

[39] F. Mehmood, M. Hoffmann, P. D. Lomenzo, C. Richter, U. Schröder, Adv. Mater. Inter. 6 (2019) 1901180.

[40] N. Gong, T. P. Ma, IEEE. Electron. Device. Lett. 37 (2016) 1123-1126.

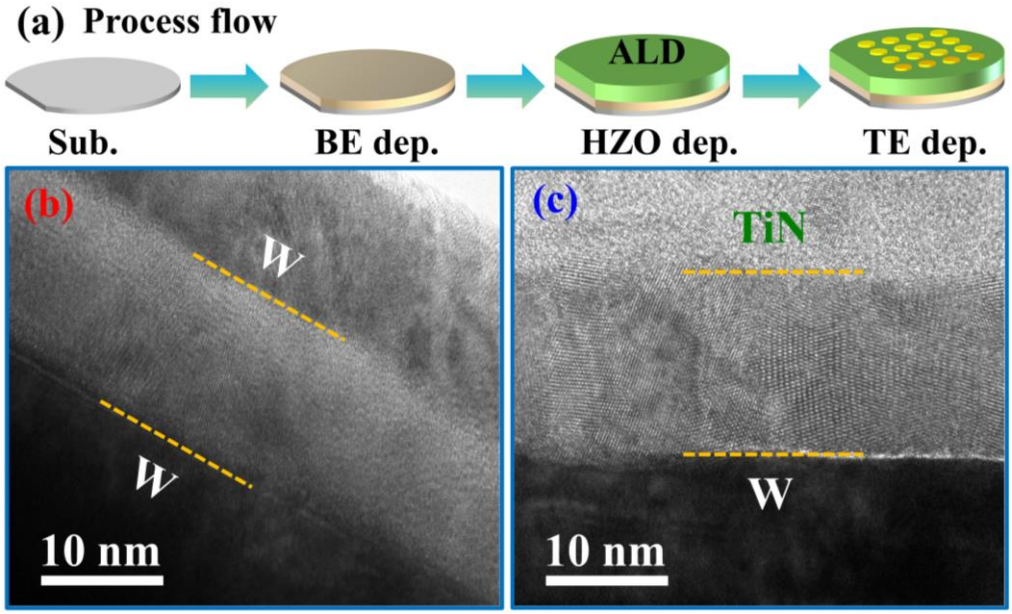

Fig. 1. (a) Process flow for the fabrication of three kinds of capacitors. Cross-sectional HRTEM images of (b) WW and (c) WT capacitors.

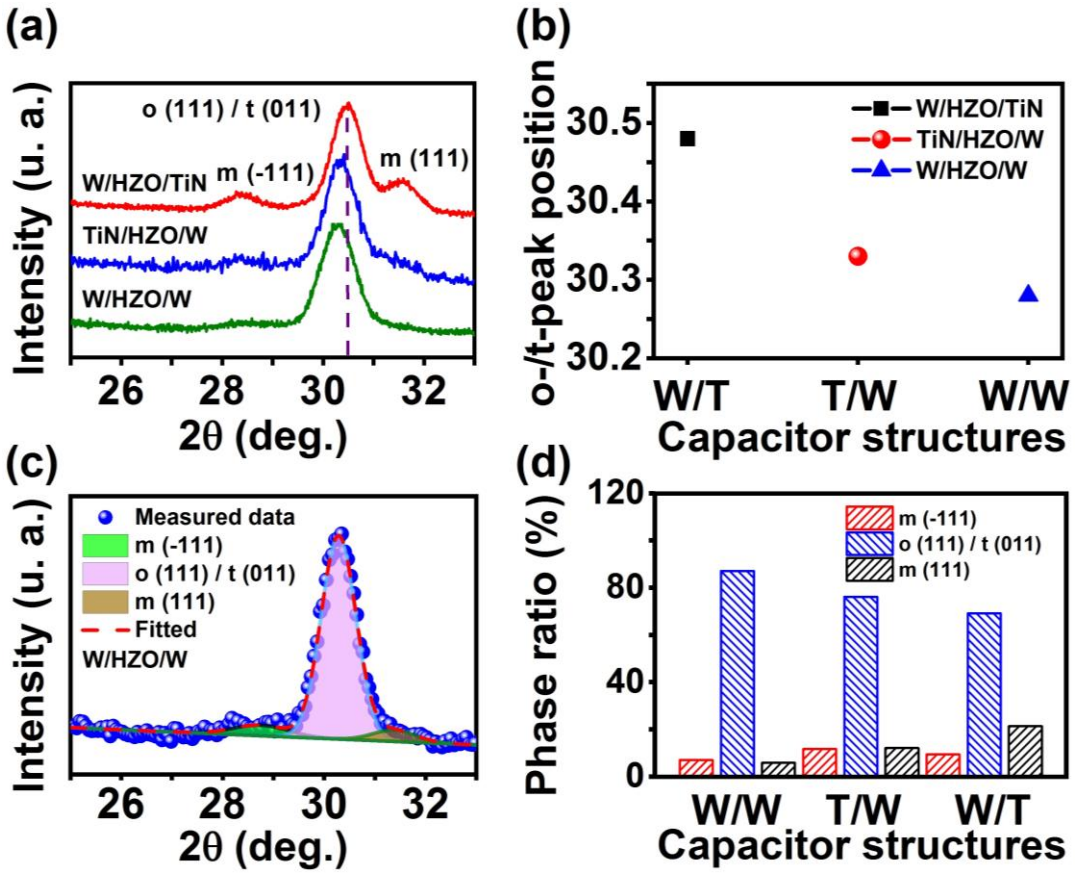

Fig. 2. (a) GIXRD patterns of three types of capacitors. (b) Evolution of o/t-peak position of HZO films with respect to the top and bottom electrodes. (c) Deconvolution of GIXRD spectra for WW capacitor. (d) Variation of the relative phase ratio of the three capacitors.

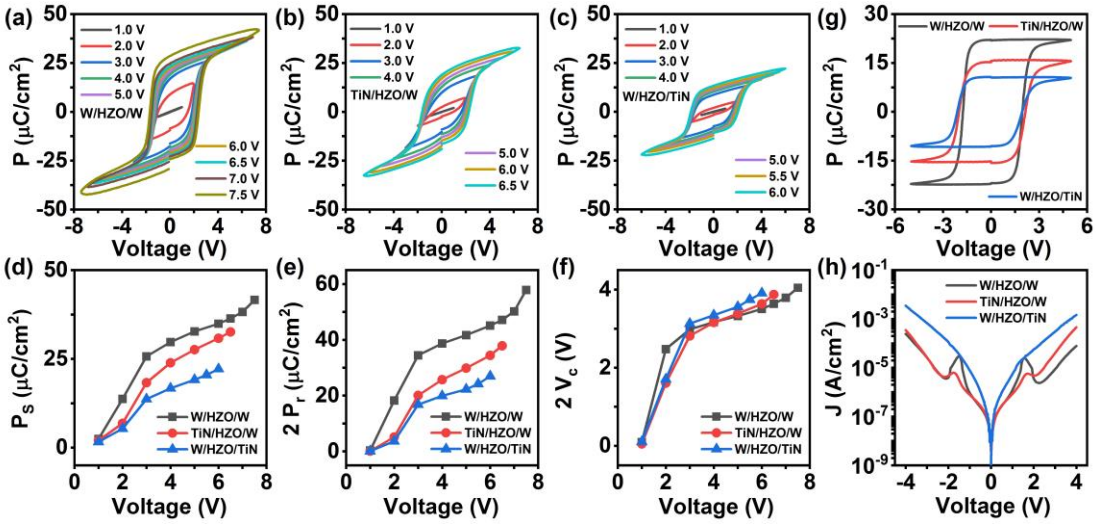

Fig. 3. Pristine P-V hysteresis loops of (a) WW, (b) TW and (c) WT capacitors. Comparison in (d) P_s, (e) 2 P_r and (f) 2 V_c between WW, TW and WT capacitors. (g) Pristine PUND loops and initial J-V curves (h) of three capacitors.

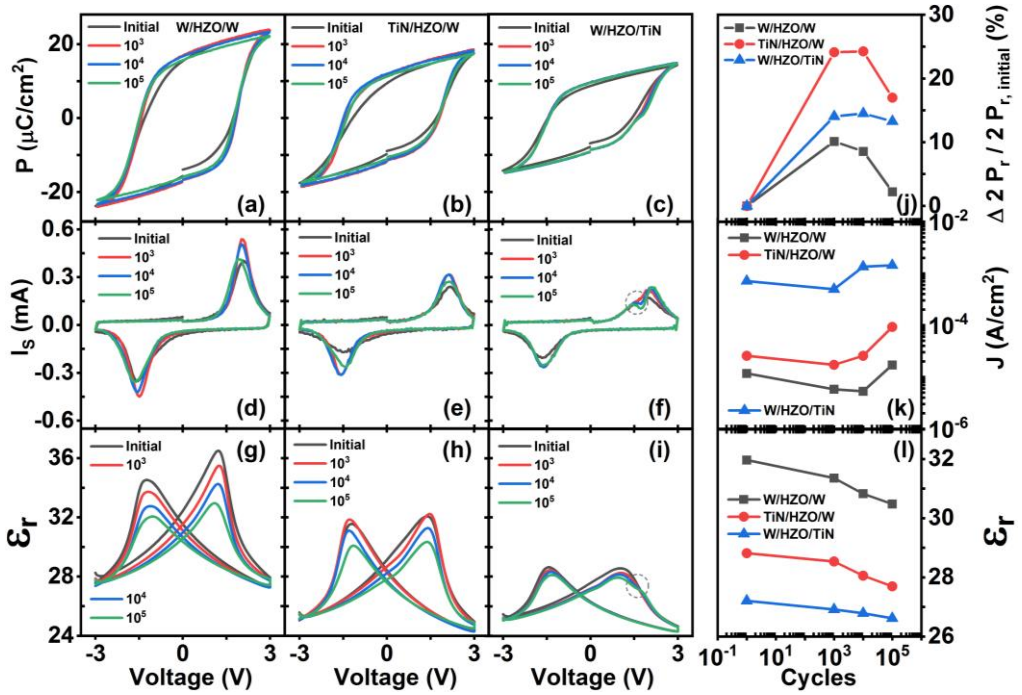

Fig. 4. The evolution of (a)-(c) P-V and (d)-(f) corresponding Is-V hysteresis loops of three capacitors subjected to 1 kHz triangle wave bipolar switching cycles with amplitude of ±3 V. (g)-(i) The change of ε_r-V curves of all the capacitors with an increase in the number of electrical switching cycles, respectively. The capacitance-voltage measurements were performed at the DC bias amplitude of ±3 V and frequency of 1.0 MHz. Summary of (j) the normalized $\Delta 2P_r/2P_{r,\,initial}$, leakage current density (k) and permittivity (l) of three capacitors as a function of the number of bipolar switching cycles.

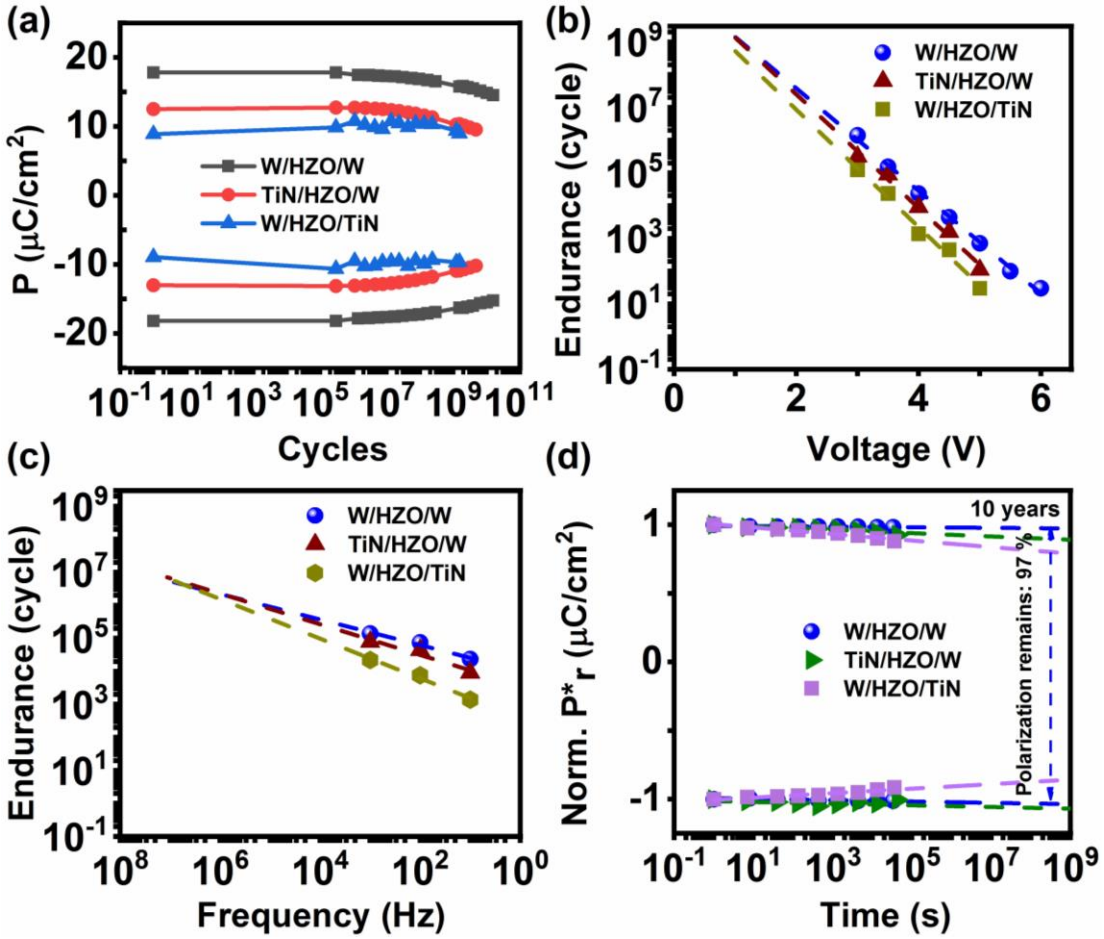

Fig. 5. (a) Endurance properties of the WW, TW and WT capacitors. Endurance characteristics with changing (b) the voltage and (c) the frequency for WW, TW and WT capacitors. (d) Retention data by extrapolating the normalized polarization versus log (time) of WW, TW, and WT capacitors.